Mechatronics and Intelligent Transportation Systems
https://www.acadlore.com/journals/MITS

Field Tests and Analyses on Running Stability of Fenghuang Medium and Low Speed Maglev Train

Yuheng Ai[1,2,3], Junqi Xu[2], Guobin Lin[2*], Xiao Liang[4], Sumei Wang[5,6], Yang Lu[5,6], Chen Chen[1,2,3]

[1] Key Laboratory of Road and Traffic Engineering of the Ministry of Education, Tongji University, 201804 Shanghai, China
[2] Maglev Transportation Engineering R&D Center, 201804 Shanghai, China
[3] College of Transportation, Tongji University, 201804 Shanghai, China
[4] Hunan Rail Transit Holding Group Co., Ltd., 410000 Changsha, China
[5] Department of Civil and Environmental Engineering, The Hong Kong Polytechnic University, Hung Hom, Kowloon, 999077 Hong Kong, China
[6] National Rail Transit Electrification and Automation Engineering Technology Research Center (Hong Kong Branch), The Hong Kong Polytechnic University, Hung Hom, Kowloon, 999077 Hong Kong, China

[*] Correspondence: Guobin Lin (12154@tongji.edu.cn)

Received: 07-30-2022 **Revised:** 08-19-2022 **Accepted:** 09-06-2022

Citation: Y. H. Ai, J. Q. Xu, G. B. Lin, X. Liang, S. M. Wang, Y. Lu, and C. Chen, "Field tests and analyses on running stability of Fenghuang medium and low speed maglev train," *Mechatron. Intell Transp. Syst.*, vol. 1, no. 1, pp. 35-46, 2022. https://doi.org/10.56578/mits010105.

Abstract: Multiple field tests were carried out on the Fenghuang medium and low speed maglev train. During the tests, the authors collected the vibration data of train carriage and suspension frames under no-load (AW0). Next, the stability of the maglev train under corresponding conditions was investigated, using indices like weighted RMS acceleration (ISO 2631) and Sperling index. Through the in-depth analyses, it was concluded that the maglev train runs smoothly, and the passengers on the train generally feel comfortable.

Keywords: Field tests; Maglev train; Stability; Time domain analysis; ISO2631

1. Introduction

In comparison to the conventional wheel-rail train, the maglev train has the advantages of low loss, low noise, and great climbing ability because of the non-contact running characteristics between the maglev train and guide rail. Maglev train technology, which is used in the sector of medium and low speed and is now evolving, has emerged as a brand-new method of intercity and even urban rail transit [1-3]. Following the Changsha Maglev Express Line's successful operation, Fenghuang County in Hunan Province is using the building of a medium and low speed maglev commercial operating line as an opportunity to grow the local tourism industry.

Medium and low speed maglev lines that have been commercially operated around the world. However, due to the inherent instability of the electromagnetic levitation, the train-track-bridge coupled vibration problem is still a key factor restricting the engineering application of medium and low speed maglev technology [1, 4, 5]. The ability to extract maglev non-stationary signals can be improved using the short-time Fourier transform approach [6]. The vehicle-rail coupling and the suspension system's control efficiency are also indirectly reflected in the vibration data. Track stiffness and vibration caused by vehicle-rail coupling were investigated by Zhang [7], Mace and Manconi [8]. To ensure that the calculation accuracy satisfies the criteria and is consistent with the actual engineering, Zhang et al. [9, 10] investigated the random vibration of the vehicle bridge coupling system and the rail coupling system. In their discussion of the nonlinear dynamic properties of maglev vehicles under track random irregularities, Chen et al. provided evidence that the suspension stability of maglev vehicles can be considerably impacted by random track abnormalities [11]. Numerous researchers have suggested various strategies to enhance the suspension system's control performance and train stability [12-15]. However, additional testing in engineering applications is still required to confirm the efficacy of these techniques. Therefore, numerous field tests were

carried out by researchers [16-19]. In the meanwhile, it is of certain significance to carry out field test in Fenghuang.

To intuitively reflect train running stability, a quantitative indicator was developed based on the collection and analysis of vibration data from train carriage and suspension frames. Besides, the current evaluation criteria for vehicle vibration comfort were adopted to reflect the stability and unique features of train operation.

2. Field Test

2.1 Test Line and Vehicle

As shown in Figure 1, the test site is in Fenghuang County, Xiangxi Tujia and Miao Autonomous Prefecture, Hunan Province, China. The line's straight and tunnel sections are where the test is primarily conducted. A medium- and low-speed maglev train made by CRRC Zhuzhou Electric Locomotive Co., Ltd. was used for the test.

Figure 1. Test line and vehicle

2.2 Test Contents

This test uses a variety of acceleration sensors to collect vibration data from the carriage and suspension frame, depending on the equipment state and test objectives. Weighted RMS acceleration (ISO 2631) and the Sperling index were utilized to examine the operating stability of the train on the basis of filtering the actual acquired data.

(1) Carriage vibration

The head carriage's front, middle, and back floors all have vibration sensors fitted to gather acceleration information. The front of the carriage has a three-way vibration sensor, the middle of the carriage has a vertical sensor, and the back of the carriage has a horizontal and vertical sensor. The running stability of the carriage under various working conditions can be examined using the gathered acceleration data. Schematic diagram of the test plan is shown in Figure 2.

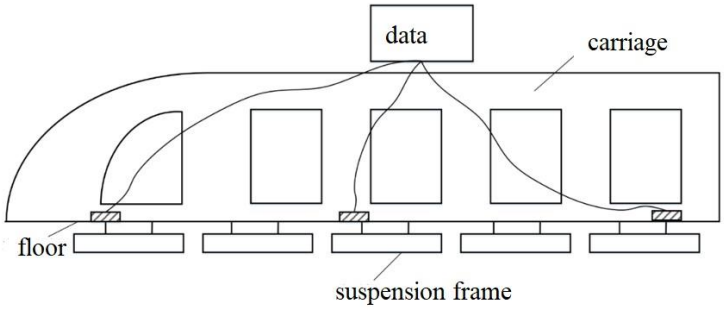

Figure 2. Test plan

(2) Vibration of suspension frame

One crucial element in controlling the suspension state of the maglev train, which is essential to the investigation of the stability of the maglev train, is the suspension frame. To get the vibration acceleration data of the suspension frame, measuring points are put on the head carriage's suspension unit and vibration sensors are installed in various directions.

(3) Running stability analysis

Weighted RMS acceleration (ISO 2631) and the Sperling index are used to generate the relevant train stability index and assess the running stability of the maglev train after collecting, filtering, and processing the vibration data of various measuring points of actual carriages.

3. Test Results

Three train conditions were considered: (1) AW0 (no-load) load condition, (2) speed limit of 20km/h, and (3) straight section operation.

3.1 Wavelet Domain Denoising

Wavelet domain denoising is mainly adopted to process data. In different scales, the wavelet generating function is translated by a distance of τ, and the translated function is multiplied by the original signal for further processing. The wavelet function can be expressed as:

$$WT_x(\alpha,\tau)=\frac{1}{\sqrt{\alpha}}\int_{-\infty}^{+\infty}x(t)\psi^*\left(\frac{t-\tau}{\alpha}\right)dt\ \alpha>0 \tag{1}$$

where, $x(t)$ is the target signal; $\psi(t)$ is the wavelet generating function; α is the scaling function; τ is the distance of translation.

The signal analysis will change into a two-dimensional space with scale domain and temporal domain when wavelet generating function is in play. To get the greatest effect, modify the frequency of position adjustments, the scale function alpha on the window's shape, and the distance of translation.

As an illustration, the Haar wavelet basis function can be defined as:

$$\psi=\begin{cases}1, & 0\le x\le\frac{1}{2}\\ -1, & \frac{1}{2}\le x\le 1\\ 0, & else\end{cases} \tag{2}$$

Its scale function can be defined as:

$$\phi=\begin{cases}1, & 0\le x\le 1\\ 0, & else\end{cases} \tag{3}$$

The Haar wavelet can be used to realize the fundamental wavelet transform. Additionally, the signal's signal to noise energy ratio typically dictates the precise number of decomposition layers.

The threshold with a good denoising impact is chosen using the model $y=f(t)+e$, where e is a white Gaussian noise that follows a N(0,1) distribution. By analyzing the wavelet coefficients, the noise in the signal is removed. Typically, the unbiased risk estimation threshold can be referred to choose the threshold.

This method involves extracting the absolute values of each element in the original signal $s(t)$ before arranging the sequence of absolute values from small to large. Finally, the resulting sorted sequence is squared to get the new signal sequence, which is denoted as $f(k)$:

$$f(k)=\left(sort(|s|)\right)^2 \tag{4}$$

Taking the threshold for $f(k)$ of the square root of the first k elements, namely, $\lambda_k=\sqrt{f(k)},(k=0,1,2,\cdots,N-1)$, then the threshold of risk can be expressed as:

$$Risk(k)=\frac{1}{N}\left[N-2k+\sum_{i=1}^{k}f(j)+(N-k)f(N-k)\right] \tag{5}$$

According to the risk function, the corresponding risk and curve can be obtained. Then, the j value corresponding to the minimum risk can be recorded as j_{min}, and the unbiased risk estimation threshold can be derived from j_{min}:

$$\lambda_k=\sqrt{f(j_{min})} \tag{6}$$

This study adopts the wavelet threshold denoising technique, which involves tailoring the denoising process to the different features of the amplitude of the signal and noise's wavelet coefficients after signal decomposition. The effect of wavelet analysis depends on the choice of wavelet basis function, number of decomposition layers,

threshold value, and threshold function. Thus, it is important to choose these factors flexibly.

In conclusion, the test data are processed using the wavelet denoising algorithm.

3.2 Carriage Vibration

Figure 3 and Figure 4 show how each component of the head carriage vibrated in the given conditions. When the train moves in the straight section, it is clear by comparing the acceleration signals of different parts that the vertical vibration amplitude is higher than the horizontal and longitudinal vibration amplitude.

The greatest acceleration of the carriage at its front during this section of driving is 0.4123 m/s^2, its middle during this section is 0.2181 m/s^2, and its rear during this section is 0.3349 m/s^2.

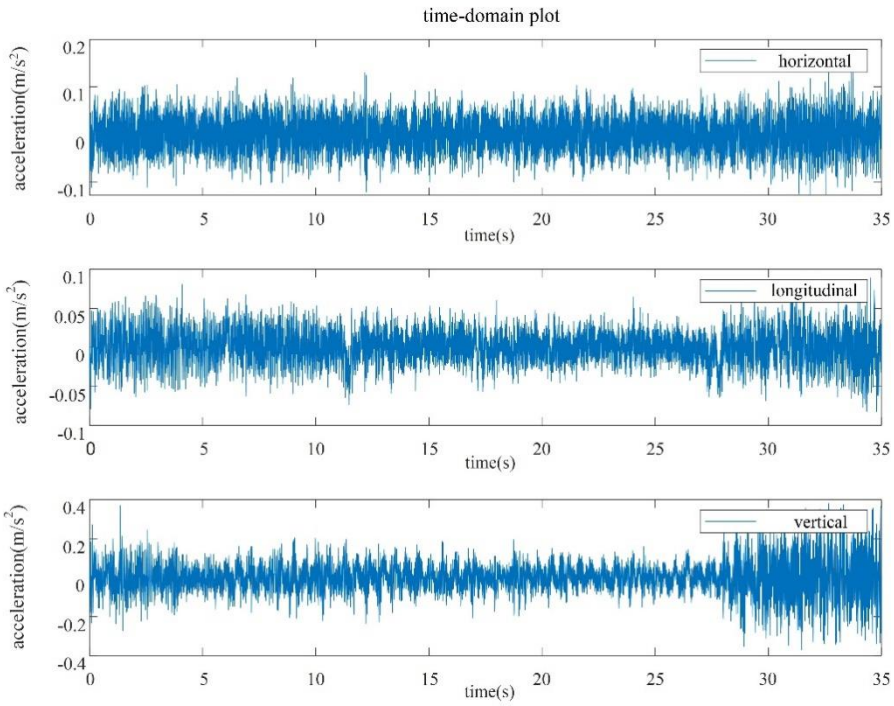

Figure 3. Vibration state of the front of the carriage in straight section

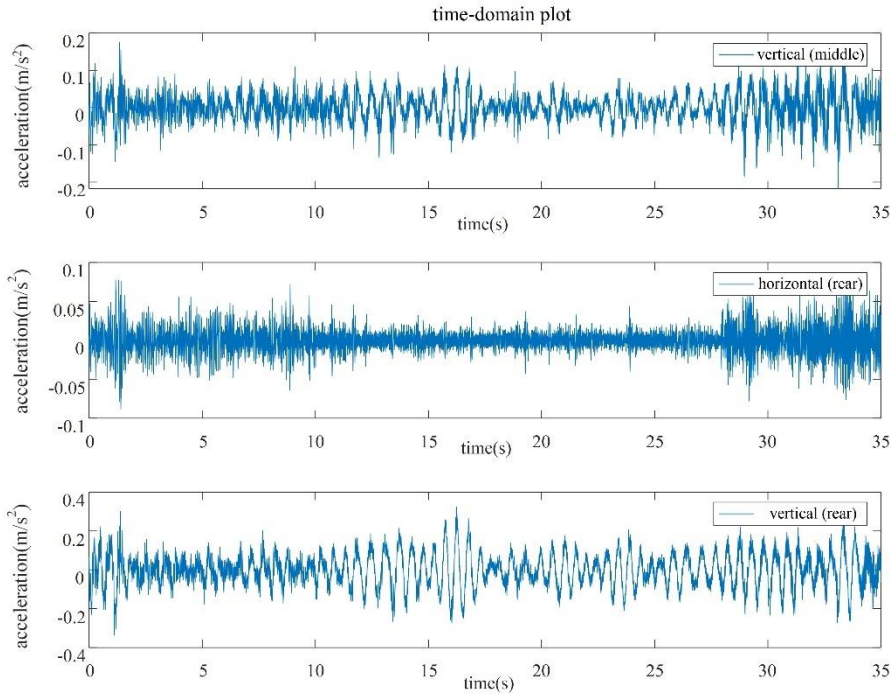

Figure 4. Vibration state of the middle and rear of the carriage in straight section

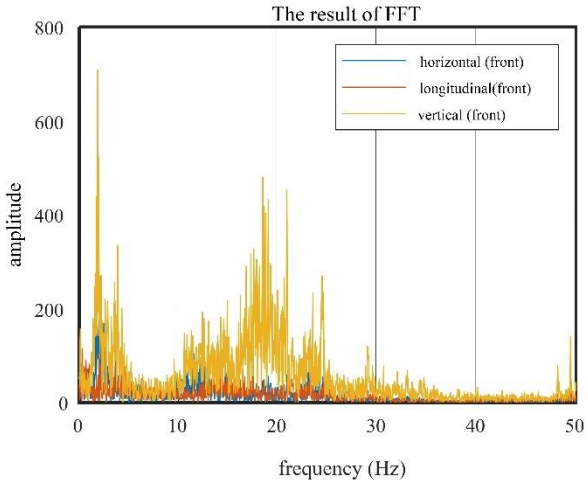

Figure 5. Frequency domain diagram of vibration in front of carriage

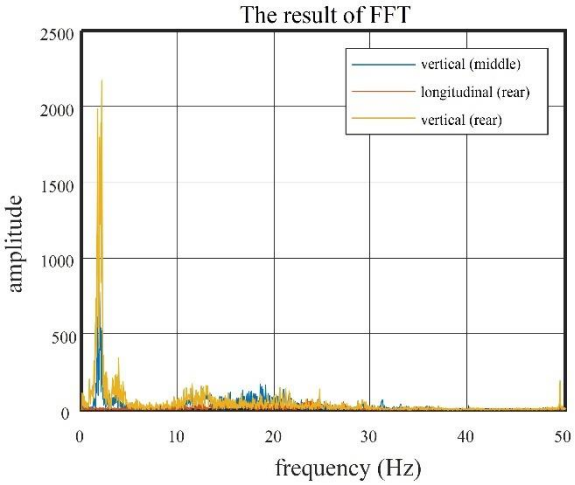

Figure 6. Frequency domain diagram of vibration in middle and rear of carriage

Figure 3 and Figure 4 illustrate how different findings are obtained at various measurement positions when the carriage vibrates in the vertical direction. It is obvious that the vertical vibration in the carriage's front is stronger than in its middle and back. A passenger may feel more stable when he/she is in the middle of the carriage because the vertical vibration amplitude in the middle of the carriage is lower than that at the front and back.

Based on this, spectral estimation and one-third frequency doubling analysis were adopted to examine the vibration acceleration obtained from each measuring point of the carriage in the frequency domain. The FFT results are shown in Figure 5 and Figure 6. The findings indicate that the carriage's vibration frequency is primarily dispersed between 0 and 30 Hz.

In addition, the first natural frequency in the horizontal vibration is approximately 1.1Hz: The level at the front is about 81dB, and that at the rear is about 69dB. The first natural frequency in the vertical vibration is roughly 2.1Hz: The level at the front, middle, and rear is 96, 90, and 102dB, respectively.

3.3 Vibration of Suspension Frame

Figures 7-10 present the acceleration changes at each measuring point of the 1#, 2# and 3# suspension frames of the head carriage, when the train is running under the setting conditions. The following conclusions can be derived from the time-domain diagrams:

1) For the same measuring point on the suspension, there is a constant variation trend in vertical, horizontal, and longitudinal vibration acceleration, with vertical acceleration having the biggest amplitude and longitudinal acceleration having the smallest. The right rear of a 2# suspension frame has a maximum vertical vibration acceleration of 1.1771 m/ s^2, the left rear of a 2# suspension frame has a maximum horizontal vibration acceleration of 3.1561 m/ s^2, and the maximum longitudinal vibration acceleration is 5.0211 m/ s^2.

2) Numerous elements, including sudden train braking, suspension control, track irregularity, etc., have an impact on the vibration of the suspension frame. The impact vibration will give an excessively large peak value in the time domain diagram. As a result, it is evident that the 2# suspension frame's left rear measuring point has a significant vibration amplitude between 20 and 22 seconds. This explains why vertical vibration has a lower maximum acceleration than horizontal and longitudinal vibration.

3) The left and right sides of the suspension frame have varied vibration accelerations, which may be due to the variable suspension controls used by the left and right sides.

4) The suspension system between the carriage and the suspension frame can effectively regulate the transmission of vibration because the vibration acceleration of the suspension frame is considerably larger than that of the carriage.

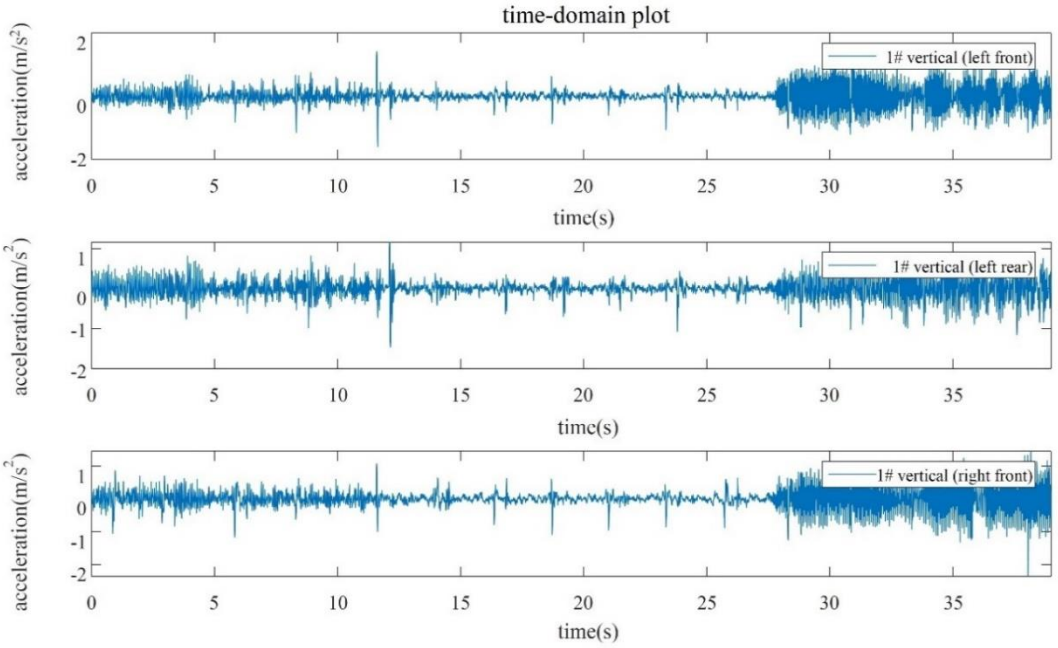

Figure 7. Vertical vibration of 1# suspension frame in straight section

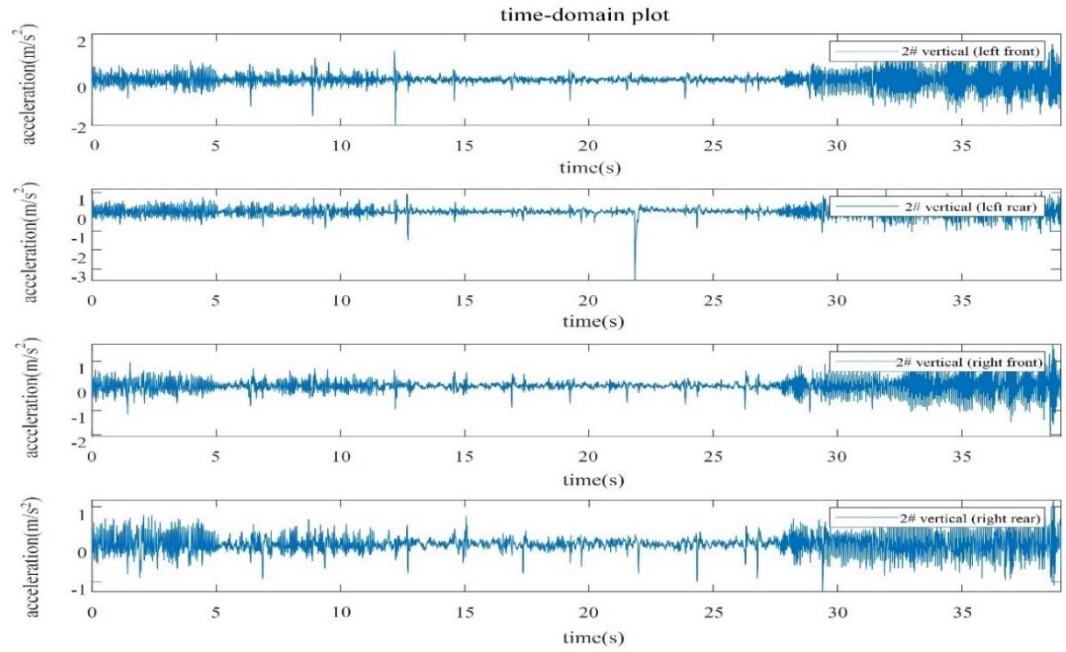

Figure 8. Vertical vibration of 2# suspension frame in straight section

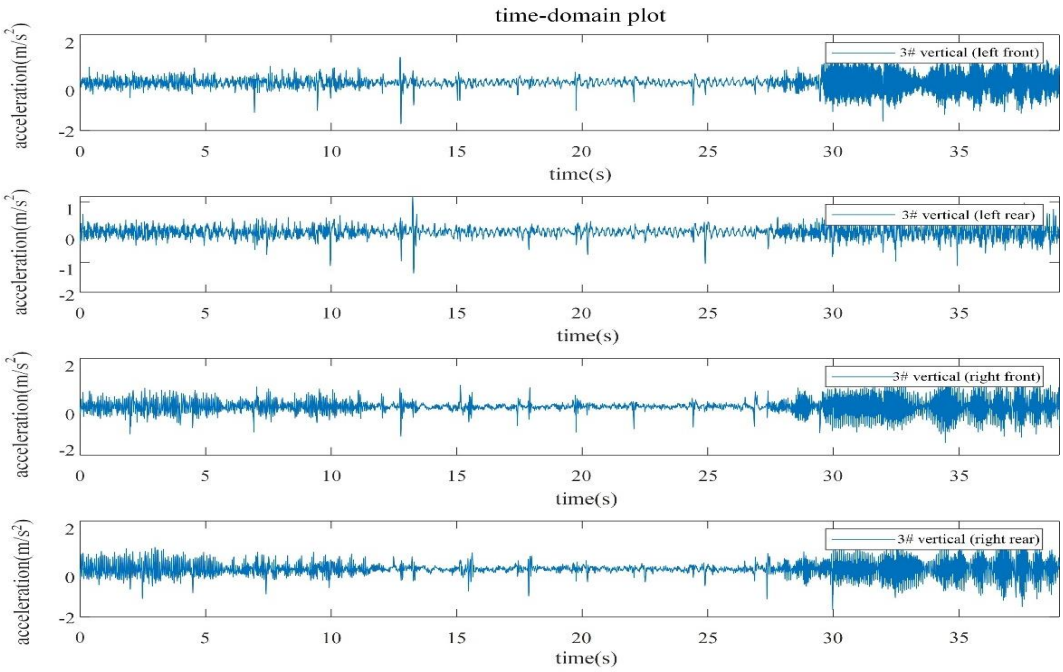

Figure 9. Vertical vibration of 3# suspension frame in straight section

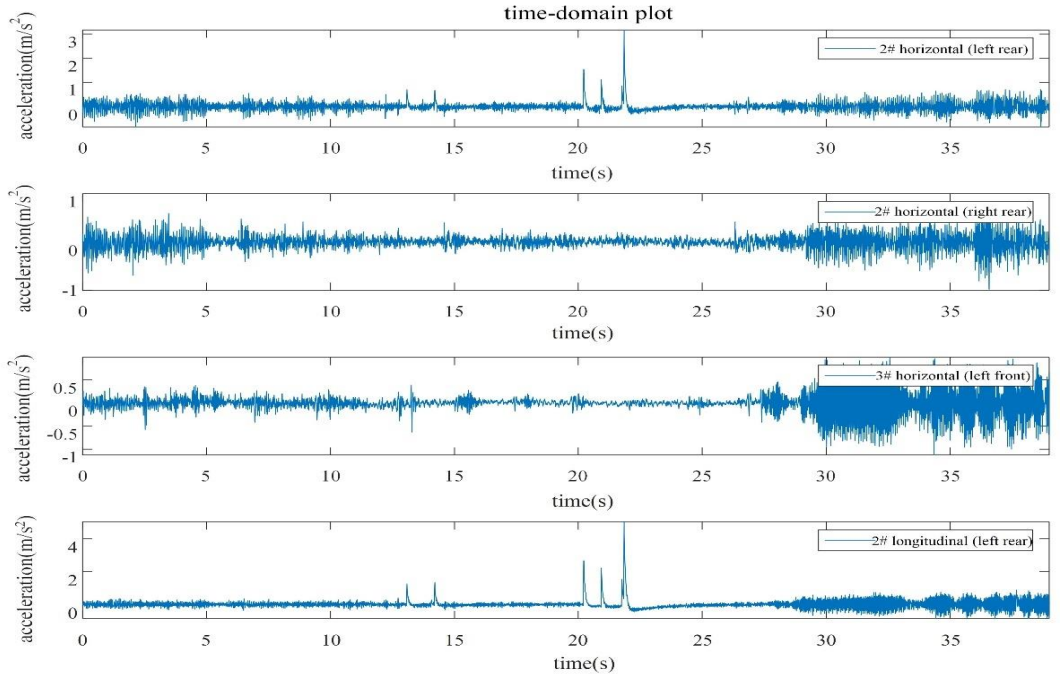

Figure 10. Horizontal and longitudinal vibrations of 2# and 3# suspension frame in straight section

The vibration acceleration of each measuring point in the suspension frame is then examined in the frequency domain, by virtue of acceleration power spectral density estimation and one-third frequency doubling analysis. The FFT results of the vibration of suspension frame are shown in Figure 11 and Figure 12. The findings demonstrate that the suspension frame's vibration is low frequency, with a vibration frequency between 0 and 40 Hz.

With the exception of the left rear measuring point of the 2# suspension frame, all measuring points of the suspension frame's horizontal vibration have essentially the same vibration frequency distribution and horizontal vibration power spectrum. Around 25.0Hz is the primary vibration frequency, while 82dB is the vibration level.

The main vibration frequency of the suspension frame is roughly 25.0Hz, and the vibration intensity is approximately 92dB. The vibration frequency distribution of the vertical vibration power spectrum is essentially the same at all measuring places.

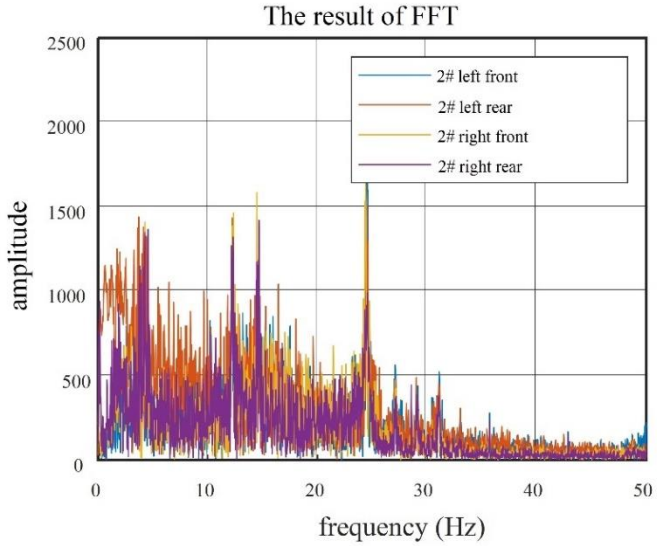

Figure 11. Vertical vibration spectrum of 2# suspension frame

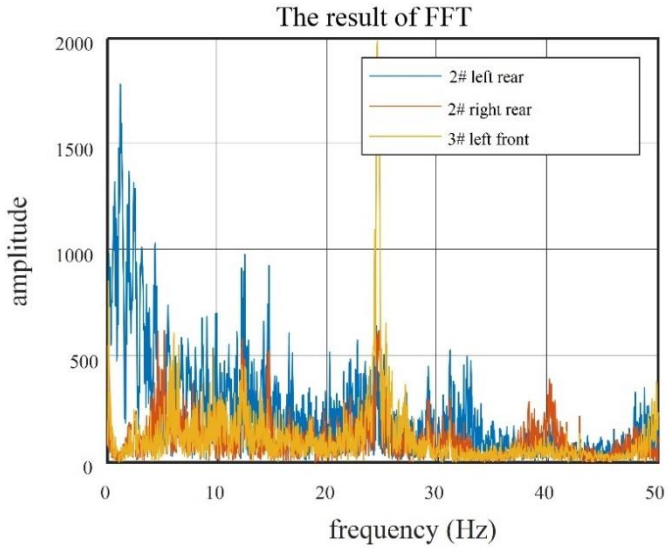

Figure 12. Horizontal vibration spectrum of 2# and 3# suspension frame

3.4 Carriage Comfort Index

Sperling carried out numerous experiments to investigate how vibration affects physiological feeling in humans. Based on the findings, they developed and suggested indicators to assess the quality of vehicle operation and passenger comfort. The Sperling stationarity assessment index has been adopted across the globe. In China, the passenger truck stability index can be calculated by:

$$W_i = 7.08 * \sqrt[10]{\frac{A_i^3}{f_i} F(f_i)} \tag{7}$$

where, A_i is vibration acceleration; f_i is vibration frequency; $F(f_i)$ is frequency correction coefficient. The value of the correction coefficient is related to the direction and frequency of vibration.

The RMS value of vibration acceleration, vibration frequency, sustained vibration time, and vibration direction are the four fundamental vibration characteristics that make up the weighted RMS acceleration (ISO 2631) approach, which is intended to describe the impact on the human body. The RMS value of the vibration acceleration of numerous different frequency bands at 1/3 octave is computed in accordance with the theory of energy addition, and the weighted value is rectified by various weighting coefficients. The effective value a_T of

weighted acceleration can be calculated by:

$$a_T = \sqrt{\sum_{1}^{n} a_i T_i} \tag{8}$$

where, a_i is the RMS of vibration acceleration at the center frequency of the i-th frequency band of 1/3 octave; T_i is the corresponding weighting coefficient.

For vertical vibration, T_i can be calculated by:

$$T_i = \begin{cases} 0.5f^2, 0.1 < f \leq 4\ Hz \\ 4/f, 4 < f \leq 8\ Hz \\ 8/f, f > 8\ Hz \end{cases} \tag{9}$$

The carriage comfort index under the test conditions were obtained from the above acceleration data (Table 1).

Table 1. Carriage comfort index (AW0, 20km/h, Straight section)

Location	ISO2631 Index	Sperling Index
Front	0.23	1.54
Middle	0.20	1.48
Rear	0.33	1.91

The established rules can be used to realize the corresponding value of weighted RMS acceleration (ISO 2631) and human subjective feelings. When the value is less than 0.315, it means that people will not feel uncomfortable; when the value is between 0.315 and 0.63, it means that people will feel slightly uneasy. When the value is larger than 0.63, it means that people will undoubtedly feel uncomfortably.

Furthermore, the Sperling index can be used to determine the carriage's stability. The level of ride comfort for passengers is evaluated as excellent when the Sperling index is less than 2.5 [20].

The aforementioned rules demonstrate that, during testing, the maglev train operates smoothly, each component of the carriage has great stability, and the human body experiences the environment as being generally comfortable.

4. Parameter Analysis

4.1 The Effect of Speed

The test was repeated under the AW0 load condition with a variable speed limit in the straight section of tracks. The speed limits were set at 20, 40, and 60km/h, respectively. The maximum carriage vibration acceleration measured for each condition is displayed in Table 2.

Table 2. Maximum vibration acceleration of carriage at different speeds (m/ s^2)

Location	20km/h	40km/h	60km/h
Front	0.4123	0.4682	0.5858
Middle	0.2181	0.1860	0.3404
Rear	0.3349	0.4359	0.8301

The three speed limiting conditions all exhibit a largely consistent variation trend in vibration acceleration. Similar to Figure 3 and Figure 4, under various speed limits, the amplitude of vertical vibration is much higher than that of horizontal and longitudinal vibration.

The impact vibration will result in an excessively high peak acceleration due to the influence of track irregularity, suspension control, and other factors throughout the testing process. However, generally speaking, as train speed increases, so does the carriage's vibration amplitude. The carriage's vibration level also increases to some amount, as shown by the results of the one-third frequency doubling analysis and spectrum estimation.

The suspension frame's vibration is essentially consistent with the previous findings and conclusions about vibration. The suspension frame's vibration amplitude increases with the running speed. At the same time, the suspension frame's vibration acceleration is still significantly greater than that of the carriage. It is obvious that the vibration transmission may be efficiently controlled by the suspension system between the carriage and the suspension frame.

4.2 Effect of Track Section

The test was repeated in the tunnel part of the tracks with an AW0 load. The speed limit is 20 km/h to allow for analysis of how different parts affect train vibration. The highest vibration acceleration of the carriage measured during the test in the tunnel portion and the straight section is displayed in Table 3 when the train is traveling at the 20 km/h speed limit.

Table 3. Maximum vibration acceleration of carriage under different section conditions (m/ s^2)

Location	Straight	Tunnel
Front	0.4123	0.4592
Middle	0.2181	0.3315
Rear	0.3349	0.7923

The carriage's vibration during the train's run in the tunnel section is not notably different from that during the straight portion. The carriage and suspension frame's vibration pattern essentially follows that of the straight section. The vibration acceleration is considerable, owing to factors such track irregularity.

4.3 Difference in Carriage Comfort Index

The relevant carriage comfort index was determined in accordance with the setting test parameters, and used to capture the variations in the index under various working conditions. Table 4 and Table 5 present the findings.

Table 4. Carriage comfort index of straight section

Location	ISO2361 index			Sperling index		
	20km/h	*40km/h*	*60km/h*	*20km/h*	*40km/h*	*60km/h*
Front	0.23	0.38	0.38	1.54	1.74	1.69
Middle	0.20	0.31	0.30	1.48	1.52	1.40
Rear	0.33	0.53	0.52	1.91	2.01	1.98

The results of the carriage comfort index test for the straight section are displayed in Table 4. It can be seen that when speed increases, the carriage's vibration level also climbs, as does the value of the carriage comfort index. This indicates that when speed increases, passengers are more likely to experience discomfort from the carriage's vibration. In addition, the center compartment's carriage comfort index is higher than that of the front and rear compartments.

The test data on carriage comfort index for the tunnel section are displayed in Table 5. The earlier data from the straight section also hold true for the operation of the tunnel section.

The straight section and the tunnel section were compared, revealing that the tunnel section is more uncomfortable. The subjective feeling of the human body was relatively comfortable, and the ride comfort for passengers in the carriage was excellent in the given circumstances, according to both indices.

Table 5. Carriage comfort index of tunnel section

Location	ISO2631 index			Sperling index		
	20km/h	*40km/h*	*60km/h*	*20km/h*	*40km/h*	*60km/h*
Front	0.21	0.29	0.31	1.68	1.75	1.83
Middle	0.18	0.25	0.26	1.58	1.79	1.63
Rear	0.30	0.39	0.42	2.15	2.40	2.20

5. Conclusions

The field tests and analysis on the running stability of the Fenghuang medium and low speed maglev train led to the following conclusions:

1) The test data for the vibration acceleration at each measuring point of the carriage and suspension frame are gathered and thoroughly examined. Comparatively, it is clear that the suspension system between the carriage and the suspension frame is capable of reducing vibration transmission efficiently.

2) Impact vibration will be triggered by elements such track irregularity, suspension control, and unexpected train braking, resulting in a significant peak acceleration of vibration.

3) The vibration amplitude of the vehicle will climb together with the increase in train operating speed, as will the vibration intensity of the vehicle.

4) The overall stability of the vehicle operation can be inferred from the outstanding ride comfort for passengers and the subjectively comfortable feeling of the human body.

Data Availability

The data used to support the findings of this study are available from the corresponding author upon request.

Conflicts of Interest

The authors declare that they have no conflicts of interest.

References

[1] H. W. Lee, K. C. Kim, and J. Lee, "Review of maglev train technologies," *IEEE T. Magn.*, vol. 42, no. 7, pp. 1917-1925, 2006. https://doi.org/10.1109/TMAG.2006.875842.

[2] Y. Sun, W. Li, H. Qiang, and D. Chang, "An experimental study on the vibration of the low-speed maglev train moving on the guideway with sag vertical curves," *Int J. Control Autom.*, vol. 9, no. 4, pp. 279-288, 2016.

[3] F. Xu, S. Luo, and Z. Deng, "Study on key technologies and whole speed range application of maglev rail transport," *J. China Railway Soc.*, vol. 41, no. 3, pp. 40-49, 2019.

[4] D. F. Zhou, C. H. Hansen, J. Li, and W. S. Chang, "Review of Coupled Vibration Problems in EMS Maglev Vehicles," *Int J. Acous. Vib.*, vol. 15, no. 1, pp. 10-23, 2010. https://doi.org/10.20855/ijav.2010.15.1255.

[5] D. X. Wang, X. Z. Li, Y. W. Wang, and Q. K. Hu, "Dynamic interaction of the low-to-medium speed maglev train and bridges with different deflection ratios: Experimental and numerical analyses," *Adv. Struct. Eng.*, vol. 23, no. 11, pp. 2399-2413, 2020. https://doi.org/10.1177/1369433220913367.

[6] W. L. Li, T. X. Chen, and R. X. Hu, "Study on running stability of maglev train," *Mech Sci. Technol. Aerospace Eng.*, vol. 38, no. 5, pp. 677-683, 2019. http://dx.doi.org/10.13433/j.cnki.1003-8728.20180238.

[7] L. L. Zhang, "Research on Hopf bifurcation and sliding mode control for suspension system of maglev train," Ph.D. Dissertation, Hunan University, China, 2010.

[8] B. R. Mace and E. Manconi, "Modelling wave propagation in two-dimensional structures using finite element analysis," *J. Sound. Vib.*, vol. 318, no. 4-5, pp. 884-902, 2008. https://doi.org/10.1016/j.jsv.2008.04.039.

[9] Y. W. Zhang, J. H. Lin, Y. Zhao, W. P. Howson, and F. W. Williams, "Symplectic random vibration analysis of a vehicle moving on an infinitely long periodic track," *J. Sound. Vib.*, vol. 329, no. 21, pp. 4440-4454, 2010. https://doi.org/10.1016/j.jsv.2010.05.004.

[10] Y. W. Zhang, J. H. Lin, and D. Kennedy, "FEM-based symplectic random vibration analysis of coupled vehicle-track systems," In 8th International Conference on Structural Dynamics, Leuven, Belgium, July 4-6, 2011, EASD, pp. 2727-2734.

[11] C. Chen, J. Q. Xu, L. J. Rong, H. L. Pan, and D. G. Gao, "Nonlinear dynamics characteristics of maglev vehicle under track random irregularities," *J. Traffic Transp. Eng.*, vol. 19, no. 4, pp. 115-124, 2019. http://dx.doi.org/10.19818/j.cnki.1671-1637.2019.04.011.

[12] Y. G. Sun, H. Y. Qiang, G. B. Lin, J. D. Ren, and W. L. Li, "Dynamic modeling and control of nonlinear electromagnetic suspension systems," *Chem. Engineer. Trans.*, vol. 46, pp. 1039-1044, 2015. https://doi.org/10.3303/CET1546174.

[13] X. Su, X. Yang, P. Shi, and L. Wu, "Fuzzy control of nonlinear electromagnetic suspension systems," *Mechatronics*, vol. 24, no. 4, pp. 328-335, 2014. https://doi.org/10.1016/j.mechatronics.2013.08.002.

[14] H. Wang, X. Zhong, and G. Shen, "Analysis and experimental study on the MAGLEV vehicle-guideway interaction based on the full-state feedback theory," *J. Vib. Control*, vol. 21, no. 2, pp. 408-416, 2015. https://doi.org/10.1177/1077546313488431.

[15] C. Chen, J. Q. Xu, G. B. Lin, Y. G. Sun, and X. Zhao, "Sliding mode bifurcation control based on acceleration feedback correction adaptive compensation for maglev train suspension system with time-varying disturbance," *IEEE T. Transp. Electr.*, vol. 8, no. 2, pp. 2273-2287, 2022. https://doi.org/10.1109/TTE.2022.3144518.

[16] M. Li, S. H. Luo, W. H. Ma, C. Lei, T. Li, Q. B. Hu, X. L. Zhang, and Y. P. Han, "Experimental study on dynamic performance of medium and low speed maglev train-track-bridge system," *Int J. Rail Transp.*, vol. 9, no. 3, pp. 232-255, 2020. https://doi.org/10.1080/23248378.2020.1798294.

[17] X. Z. Li, D. X. Wang, D. J. Liu, L. F. Xin, and X. Zhang, "Dynamic analysis of the interactions between a low-to-medium-speed maglev train and a bridge: Field test results of two typical bridges," *P I Mech. Eng. F-J. Rai.*, vol. 232, no. 7, pp. 2039-2059, 2018. https://doi.org/10.1177/0954409718758502.

[18] Y. F. Song, G. B. Lin, F. Ni, J. Q. Xu, and C. Chen, "Study on coupled vertical vehicle-bridge dynamic performance of medium and low-speed maglev train," *Appl. Sci.*, vol. 11, no. 13, pp. 5898-5898, 2021.

https://doi.org/10.3390/app11135898.
[19] M. D. Zhai, Z. Q. Long, and X. L. Li, “Calculation and evaluation of load performance of magnetic levitation system in medium-low speed maglev train,” *Int J. Appl. Electrom.*, vol. 61, no. 4, pp. 519-536, 2019. https://doi.org/10.3233/JAE-190031.
[20] Z. G. Deng, J. P. Li, W. H. Ma, Y. F. Gou, Y. Ren, and J. Zheng, “High-Temperature superconducting magnetic levitation vehicles: Dynamic characteristics while running on a ring test line,” *IEEE Veh. Technol. Mag.*, vol. 12, no. 3, pp. 95-102, 2017. https://doi.org/10.1109/MVT.2017.2700493.